Journal of Power Sources 186 (2009) 305–310

Contents lists available at ScienceDirect

Journal of Power Sources

journal homepage: www.elsevier.com/locate/jpowsour

Structural and electrochemical studies of $Ba_{0.6}Sr_{0.4}Co_{1-y}Ti_yO_{3-\delta}$ as a new cathode material for IT-SOFCs

Hailei Zhao[a,c,*], Deqiang Teng[a], Xiuhua Zhang[b], Cuijuan Zhang[a], Xue Li[a]

[a] Department of Inorganic Nonmetallic Materials, School of Materials Science and Engineering, University of Science and Technology Beijing, Beijing 100083, China
[b] Central Research Institute of Building and Construction, MCC Group, Beijing 100088, China
[c] Beijing Key Lab of New Energy Material and Technology, Beijing 100083, China

ARTICLE INFO

Article history:
Received 5 September 2008
Received in revised form 2 October 2008
Accepted 2 October 2008
Available online 15 October 2008

Keywords:
$Ba_{0.6}Sr_{0.4}Co_{1-y}Ti_yO_{3-\delta}$
Cathode
Electrical conductivity
Thermal expansion
SOFC

ABSTRACT

The influence of titanium doping level in $Ba_{0.6}Sr_{0.4}Co_{1-y}Ti_yO_{3-\delta}$ (BSCT) oxides on their phase structure, electrical conductivity, thermal expansion coefficient (TEC), and single-cell performance with BSCT cathodes has been investigated. The incorporation of Ti can lead to the phase transition of $Ba_{0.6}Sr_{0.4}CoO_{3-\delta}$ from hexagonal to cubic structure. The solid solution limitation of Ti in $Ba_{0.6}Sr_{0.4}Co_{1-y}Ti_yO_{3-\delta}$ is 0.15–0.3 under 1100 °C. BSCT shows a small polaron conduction behavior and the electrical conductivity increases steadily in the testing temperature range (300–900 °C), leading to a relatively high conductivity at high temperatures. The electrical conductivity decreases with increasing Ti content. The addition of Ti deteriorates the cathode performance of BSCT slightly but decreases the TEC significantly. The TEC of BSCT is about 14×10^{-6} K^{-1}, which results in a good physical compatibility of BSCT with $Gd_{0.2}Ce_{0.8}O_{2-\delta}$ (GDC) electrolyte. BSCT also shows excellent thermal cyclic stability of electrical conductivity and good chemical stability with GDC. These properties make BSCT a promising cathode candidate for intermediate temperature solid oxide fuel cells (IT-SOFCs).

1. Introduction

The solid oxide fuel cell (SOFC) is one of the most realistic candidates for a new generation power system due to its higher efficiency and fuel flexibility [1]. However, the current state of the art SOFC still has many problems related to its longevity or long term stability due to its high operation temperature of around 1000 °C [2]. Thus, the reduction of operating temperature is a critical issue in SOFC, and the majority of current researches is concentrated on the development of intermediate temperature SOFCs (IT-SOFCs) that can be operated below 800 °C [3]. The decrease of operating temperature, however, leads to a significant decrease in electrode activity, especially for the conventional SOFC cathode, strontium-doped lanthanum manganite (LSM) [4–7]. It shows low electrical conductivity and poor catalytic activity below 800 °C and thus not suitable for IT-SOFCs. So it is necessary to find new cathode material to enhance the performance of IT-SOFCs.

Cobalt-based perovskite compounds (ABO_3) have attracted a lot of attention as an IT-SOFCs cathode due to their mixed-conducting characteristics and higher ion-conductivity in the intermediate temperature range [8–16]. The mixed conductivity extends the active oxygen reduction site from the typical electrolyte-electrode-gas triple-phase boundary to the entirely exposed cathode surface, therefore greatly reducing the cathode polarization at low operating temperatures. Among those perovskite-type mixed conducting oxides, $Ba_{0.5}Sr_{0.5}Co_{0.8}Fe_{0.2}O_{3-\delta}$ (BSCF5582) composite shows great potential as a cathode material and has received considerable attentions in recent years [17–22]. Although very promising results were reported, there are still some disadvantages, such as the high thermal expansion coefficient (TEC) as large as $19–24 \times 10^{-6}$ K^{-1} [23–25] and the poor chemical compatibility with CeO_2-based electrolytes [23,26]. From the viewpoint of SOFC applications, the good chemical compatibility and the matched TEC of the cathode with electrolyte is crucial for the operation stability of SOFCs.

In general, the larger TEC values observed with the cobalt-based perovskite compounds can be attributed to the electronic spin state transitions associated with the Co^{3+} ions and the formation of oxide ion vacancies [27,28]. The replacement of Co by more stable Ti ions is expected to decrease the TEC of the compounds and improve the chemical stability with CeO_2-based materials. Our previous study showed that the cathode performance of $Ba_{0.6}Sr_{0.4}Co_{0.8}Fe_{0.2}O_{3-\delta}$ is better than that of $Ba_{0.5}Sr_{0.5}Co_{0.8}Fe_{0.2}O_{3-\delta}$ [29]. In this contribution, $Ba_{0.6}Sr_{0.4}Co_{1-y}Ti_yO_{3-\delta}$ (BSCT) was prepared to investigate the effect of Ti content on the properties of BSCT, including

* Corresponding author at: School of Materials Science and Engineering, University of Science and Technology Beijing, Beijing 100083, China. Tel.: +86 10 82376837; fax: +86 10 82376837.
E-mail address: hlzhao@mater.ustb.edu.cn (H. Zhao).

0378-7753/$ – see front matter © 2008 Elsevier B.V. All rights reserved.
doi:10.1016/j.jpowsour.2008.10.007

electrical conductivity, thermal expansion coefficient, chemical compatibility with CeO_2-based electrolyte, as well as cell performance.

2. Experimental

2.1. Powder synthesis and sample preparation

A conventional solid-state reaction synthesis method with high purity $BaCO_3$, $SrCO_3$, TiO_2 and $C_4H_6CoO_4{\cdot}4H_2O$ as starting materials was used to prepare $Ba_{0.6}Sr_{0.4}Co_{1-y}Ti_yO_{3-\delta}$ ($y = 0.10$–0.35) cathode materials. Required amounts of the starting materials were mixed and fired in air at 900 °C for 10 h. The so-obtained powders were ground slightly to destroy agglomerates, mixed with 2 wt% PVA (polyvinyl alcohol) as binder and then pressed into bars (40 mm × 7 mm × 3 mm) by uniaxially pressing (ca. 150 MPa). The green bars were sintered at 1100 °C for 10 h to get dense samples. Sintered bars were polished for density and electrical conductivity measurements.

2.2. Cell preparation

Single-cells consisting of porous BSCT cathode and a dense $Gd_{0.2}Ce_{0.8}O_{2-\delta}$ (GDC) electrolyte were fabricated. Uniaxially pressed (ca. 115 MPa) disks of GDC were sintered at 1550 °C for 10 h in air to obtain the dense GDC electrolyte. BSCT electrodes with active area of 0.5 cm^2 were screen printed on one side of GDC electrolyte disks with a diameter of 12 mm and a thickness of 300 μm. The electrode pastes were prepared by mixing the 1100 °C-calcined BSCT powder with carbon powder as the pore-forming reagent and ethylic cellulose solution. Then, the pastes were screen-printed twice on the same side of the electrolyte disk, followed by sintering at 850 °C for 0.5 h and 900 °C for 5 h respectively after printing. A current collector platinum layer was further coated onto each side of the single-cell and calcined at 800 °C for 0.5 h.

2.3. Characterization

The crystal structure of synthesized powders was characterized by X-ray diffraction (XRD, Rigaku D/max-A X-ray) using Cu $K\alpha_1$ radiation. The relative density of BSCT pellet was about 90%, as measured by the standard Archimedes method using distilled water as medium. Sintered bars for conductivity measurements were wrapped with four Pt wires which were held in place by small notches cut on the sample surfaces. Electrical conductivity was measured using the four-terminal method from 300 to 900 °C in air. The electrical power was supplied by a constant voltage/current source and the current and voltage drop were monitored by potentiometer (±0.1 mV) and ampere meter (±0.01 mA). All measurements were taken after holding at each temperature to equilibrate for at least 15 min when no significant change in conductivity was observed. To examine the compatibility of BSCT with GDC, the 1100 °C-fired BSCT was mixed with GDC in the weight ratio of 1:1, followed by uniaxially pressing (ca. 150 MPa) and sintering at different temperatures. The sintered pellets were crushed and examined by XRD to identify the phases present. Thermal expansion coefficient of the samples was measured in the temperature range of 50–1050 °C, using standard dilatometry technique (Netzsch DIL 402 PC). The heating rate for dilatometry measurements was 3 °C min^{-1}.

I–V and *I–P* curves which were used to characterize the single-cells performance were collected using a HP 3468A multimeter to get the voltage and a UNI-T UT60A amperemeter to get the current. H_2 saturated with room temperature water was fed into the anode chamber as fuel at a flow rate of 50 ml min^{-1} (STP) and static air was used as oxidant gas for the cathode chamber. Gas flow rates were controlled by mass flow controllers.

3. Results and discussion

3.1. Crystal structure

$BaCoO_{3-\delta}$ and $SrCoO_{3-\delta}$ usually show hexagonal structure [30]. For perovskite $ACoO_3$ compounds with A-site co-occupied by Ba and Sr, for example, $Ba_{0.5}Sr_{0.5}CoO_{3-\delta}$, the obtained structure is still hexagonal perovskite [29]. In order to achieve cubic perovskite structure to ensure the excellent oxygen ion transportation performance [31], other metal ions with more stable oxidation valence state were introduced to replace partial Co content, e.g. $Ba_{0.5}Sr_{0.5}Co_{0.8}Fe_{0.2}O_{3-\delta}$ and $BaCo_{0.7}Fe_{0.3-x}Nb_xO_{3-\delta}$ [17–19,32]. Fig. 1 shows the X-ray diffraction (XRD) patterns of the $Ba_{0.6}Sr_{0.4}Co_{1-y}Ti_yO_{3-\delta}$ powders calcined at 1100 °C. The introduction of Ti-ions could apparently make the materials exist in cubic perovskite structure. A 0.1 mol Ti-ion in $Ba_{0.6}Sr_{0.4}Co_{1-y}Ti_yO_{3-\delta}$ was, however, insufficient. A certain amount of hexagonal phase still remained. Single-phased powders with a cubic ABO_3 perovskite-type structure were obtained when $0.15 \le y \le 0.3$.

The structure type of perovskite compound is usually determined by the tolerance factor *t*, as described in Eq. (1).

$$t = \frac{r_A + r_O}{\sqrt{2}(r_B + r_O)} \quad (1)$$

where r_A, r_B and r_O correspond to the effective ionic radius of the lattice constituents. When $t = 1$, the material reaches a standard cubic perovskite structure. The cubic phase can be maintained with $0.95 \le t \le 1.04$, while orthorhombic and hexagonal phases will be obtained when $0.75 < t < 0.9$ and $t > 1.04$, respectively [33]. According to the ionic radius from literature [34], the tolerance factor *t* for compound $Ba_{0.5}Sr_{0.5}CoO_{3-\delta}$ is much higher than 1 regardless of the valence state of Co-ion (by Co^{3+} and/or Co^{4+}), which thus results in the hexagonal type structure of $Ba_{0.5}Sr_{0.5}CoO_{3-\delta}$. The ionic radii involved in this study are listed in Table 1. Based on Eq. (1), doping on B-site with large ions has the possibility to decrease the tolerance factor, and thus making the materials exist in cubic structure. Ti^{4+} has a relatively large size, 0.0605 nm, hence the replacement of Ti for Co in $Ba_{0.6}Sr_{0.4}Co_{1-y}Ti_yO_{3-\delta}$ could lead to the existence of cubic perovskite structure. Because the titanate-based perovskite usually needs high temperature to synthesize and densify due to their high melting point and low diffusion coefficient. With increasing Ti content in $Ba_{0.6}Sr_{0.4}Co_{1-y}Ti_yO_{3-\delta}$, the synthesis temperature

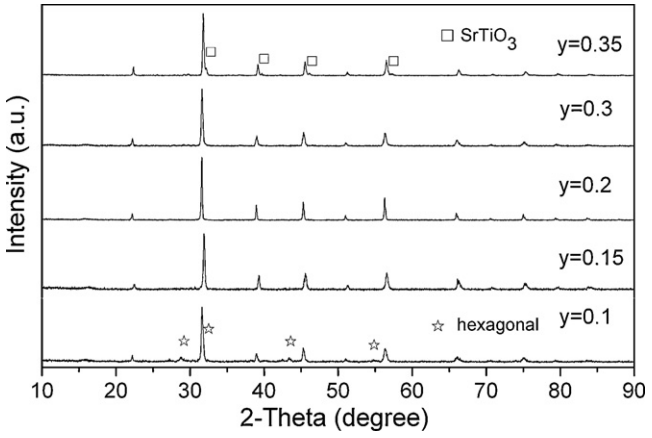

Fig. 1. XRD patterns of $Ba_{0.6}Sr_{0.4}Co_{1-y}Ti_yO_{3-\delta}$ after fired at 1100 °C for 10 h in air.

Table 1
Ionic radii involved in $Ba_{0.6}Sr_{0.4}Co_{1-y}Ti_yO_{3-\delta}$ compound [34].

Ion	Coordination number	Ionic radius (nm)
O^{2-}	6	0.14
Ba^{2+}	12	0.161
Sr^{2+}	12	0.144
Co^{3+}(LS)	6	0.0545
Co^{4+}	6	0.053
Ti^{4+}	6	0.0605

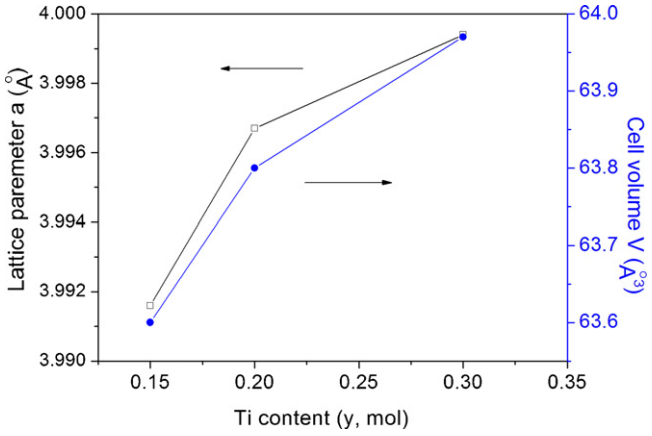

Fig. 2. Lattice constant and cell volume as a function of Ti content in $Ba_{0.6}Sr_{0.4}Co_{1-y}Ti_yO_{3-\delta}$.

may be increased. The 0.3 mol Ti should be the upper limitation for $Ba_{0.6}Sr_{0.4}Co_{1-y}Ti_yO_{3-\delta}$ at 1100 °C.

It can be seen that the main peaks for BSCT shift gradually to the lower angle direction with the increasing content of Ti in the materials. The shift to lower angle direction, corresponding to a lattice expansion, is due to the larger ionic radius of Ti compared with Co. The lattice parameters and unit cell volumes calculated by Rietveld refinement method are plotted in Fig. 2. It is obvious that both of them increase constantly with increasing Ti content.

3.2. Electrical conductivity

The temperature dependence of the total electrical conductivity of BSCT samples is shown in Fig. 3. The electrical conductivity increased with increasing temperature in air within the whole

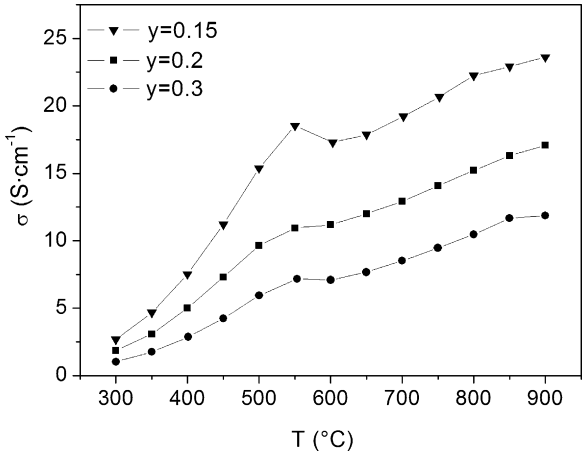

Fig. 3. Electrical conductivity of $Ba_{0.6}Sr_{0.4}Co_{1-y}Ti_yO_{3-\delta}$ as a function of temperature.

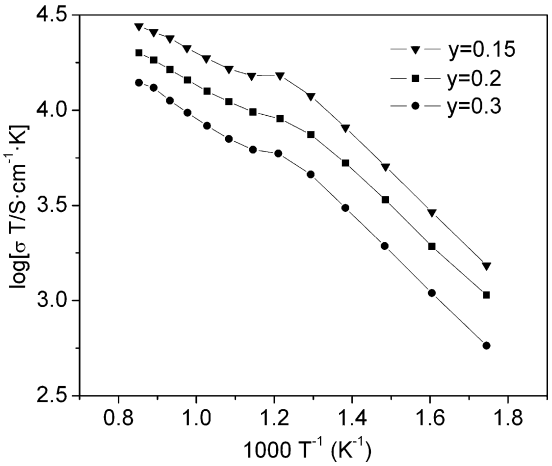

Fig. 4. $\log \sigma T$ versus $1000/T$ in air for $Ba_{0.6}Sr_{0.4}Co_{1-y}Ti_yO_{3-\delta}$.

investigated temperature range, showing a positive temperature coefficient. No maximum electrical conductivity was found for all the investigated samples in the temperature range of 300–900 °C. While many p-type mixed conductors showed electrical conductivity change with a maximum value, such as $Ba_{0.5}Sr_{0.5}Co_{0.8}Fe_{0.2}O_{3-\delta}$ [30], $Pr_{1-x}Sr_xCo_{0.2}Fe_{0.8}O_{3-\delta}$ [34] and $La_{0.8}Sr_{0.2}Co_{1-y}Fe_yO_{3-\delta}$ [35]. The logarithm of electrical conductivity versus reciprocal temperature of different BSCT compositions is shown in Fig. 4. At low temperatures, there was a good linear relationship for all investigated samples, indicating the thermally activated small-polaron conduction behavior of BSCT.

The temperature dependence of electrical conductivity for semiconductors can be described by:

$$\sigma = \left(\frac{A}{T}\right) \exp\left(\frac{-E_a}{kT}\right) \tag{2}$$

where A is the material constant containing the carrier concentration term, E_a is the activation energy for hopping conduction, k is Boltzmann's constant and T is the absolute temperature. The term A will be a constant if the charge carrier concentration is constant over the temperature range studied. Two different temperature dependences of electrical conductivity are expected. The exponential term, $\exp(-E_a/kT)$, and the pre-exponent factor, (A/T), will result in the electrical conductivity increasing at low temperature and decreasing at high temperatures, respectively, with increasing temperature. The maximum electrical conductivity will be achieved at temperature:

$$T_{max} = \frac{E_a}{k} \tag{3}$$

From the linear part of Fig. 4, the activation energy of BSCT for small polaron conduction can be calculated. They were ca. 0.17 ± 0.008 eV for $Ba_{0.6}Sr_{0.4}Co_{1-y}Ti_yO_{3-\delta}$ ($y = 0.15$–0.3). Accordingly, the transition temperatures for electrical conductivity were ca. 1973 K based on Eq. (3), which are too high to excess the temperature range investigated, thus leading to the steadily rise of electrical conductivity in the testing temperature range. On the other hand, the lattice oxygen loss of p-type semi-conductors at high temperatures would also cause the decrease of electrical conductivity due to the reduction of charge carrier concentration (electron holes), as expressed by Eq. (4):

$$2Co_{Co}^{\bullet} + O_O^{\times} \rightarrow 2Co_{Co}^{\times} + V_O^{\bullet\bullet} + \tfrac{1}{2}O_2(g) \tag{4}$$

where $Co_{Co}^{\bullet}$ refers to Co^{4+} localized on Co^{3+}-site and $Co_{Co}^{\times}$ stands for Co^{3+}. $O_O^{\times}$ is lattice oxygen and $V_O^{\bullet\bullet}$ represents oxygen vacancy.

This will result in the decrease of electrical conductivity to occur in advance, namely, the practical transition temperature for electrical conductivity decrease is much lower than the calculated one (T_{max}), as observed in literatures [30,36,37]. However, there was only an electrical conductivity fluctuation for BSCT at ca. 550 °C, corresponding also to the lattice oxygen loss of materials [37,38], no permanent decrease of electrical conductivity was observed in the test temperature range, indicating the little lattice oxygen loss and thus relatively good structural stability of BSCT. The fluctuation of conductivity became obscure with increasing Ti content. The lattice oxygen loss will result in the decrease of electronic charge carrier concentration [$Co_{Co}^{\bullet}$] and the increase of oxygen vacancy concentration [$V_O^{\bullet\bullet}$], according to Eq. (4). The little lattice oxygen loss, thus, produces small amount of oxygen vacancy, which is beneficial to the suppression of the thermal expansion coefficient of materials. This will be discussed in detail in Section 3.3.

The electrical conductivity of BSCT decreased with increasing Ti content. For BSCT, the electrical conductivity depends on the concentration of charge carriers, i.e. [$Co_{Co}^{\bullet}$]. The substitution of Ti for Co resulted in the decrease of [Co^{4+}] due to the stable valence state of Ti^{4+} in oxidizing atmosphere, and thus leading to the decrease of electrical conductivity with Ti content in BSCT. Nevertheless, BSCT showed a steadily increasing tendency of electrical conductivity with temperature rather than BSCF with a maximum conductivity value; therefore, they possessed relatively high electrical conductivity at high temperature range, which is desirable by the SOFCs.

After the temperature corresponding to the lattice oxygen loss (550 °C), the electrical conductivity increased at a reduced rate, but still with a linear relationship in Arrhenius plots (Fig. 4), suggesting that the conduction behavior was still controlled by the small polaron hopping process. The activation energy E_a was ca. 0.11 ± 0.005 eV, which was apparently lower than that at low temperatures. The decreased E_a should come from the defect dissociation between the positive and negative defects due to the decrease of electronic defect concentration [39,40]. For a system with low defect concentration, the average distance between defects is relatively long and thus resulting in weak interaction between these defects. This will lead to lower thermal activation energy for defect migration, including the hopping process of electron holes.

For the repeated start-up process of SOFCs, the thermal-cyclic performance of cathode material is of great importance for cell operation durability. Sample $Ba_{0.6}Sr_{0.4}Co_{0.8}Ti_{0.2}O_{3-\delta}$ was subjected to thermal cyclic examination, during which the electrical conductivity was recorded. The process of heating a sample to each designated temperatures for electrical-conductivity measurement and then cooling down to room temperature in a furnace is defined as the 1st cycle. For the same sample, the following repeated process is defined as 2nd cycle. Fig. 5 shows the cyclic electrical conductivity of $Ba_{0.6}Sr_{0.4}Co_{0.8}Ti_{0.2}O_{3-\delta}$ as a function of temperature. BSCT have good conductivity stability, there was no distinct decay after repeated test of electrical conductivity. This result also demonstrates the good structure stability of BSCT materials. A good thermal stability of conductivity and structure of BSCT is desired when applied as SOFC cathode.

3.3. Thermal expansion coefficient

The thermal expansion measurements for BSCT were carried out in the temperature range of 50–1050 °C. The thermal expansion curves are shown in Fig. 6. They show linear dependences with temperature in the range of 50–550 °C and 550–1050 °C, respectively. There is a turning point at 550 °C, after which the curves go fast with increasing temperature. This temperature corresponds to the transition temperature of electrical conductivity (Fig. 3), where lattice oxygen begins to lose and thus resulting in the severe lattice expansion. The linear thermal expansion coefficients in high temperature range are $16.7 \times 10^{-6}\,K^{-1}$ and $15.9 \times 10^{-6}\,K^{-1}$ for $y = 0.15$ and $y = 0.2$ samples, respectively. The average TECs in whole temperature range are $14.3 \times 10^{-6}\,K^{-1}$ for $y = 0.15$ and $13.6 \times 10^{-6}\,K^{-1}$ for $y = 0.2$, respectively. They are much smaller than the reported values for BSCF [23–25] and very close to that of GDC electrolyte ($12 \times 10^{-6}\,K^{-1}$ approximately [41]), demonstrating that Ti-doping can decrease the TEC of cobalt-based perovskite materials significantly.

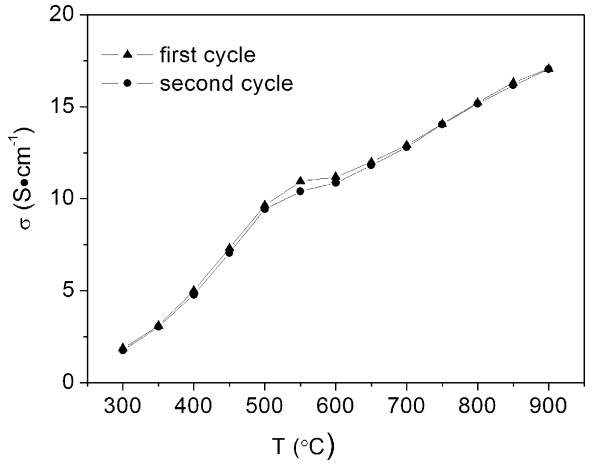

Fig. 5. Thermal cyclic performance of electrical conductivity of $Ba_{0.6}Sr_{0.4}Co_{0.8}Ti_{0.2}O_{3-\delta}$ as a function of temperature.

Generally, cobalt-based perovskite oxides exhibited large TEC values, which is attributable to the electronic spin state transitions associated with the Co^{3+} [27]. Co^{3+} ions will transform from the low-spin state t_{2g}^6 to high-spin state $t_{2g}^4 e_g^2$ with increasing temperature, and the ionic radius is larger for high-spin state compared to the low-spin state. On the other hand, Ti^{4+} ions are much stable at high temperatures, while the Co^{4+} ions are apt to be reduced to Co^{3+} ions with the generation of corresponding amount of oxide ion vacancies. Both the formation of Co^{3+} with large size than Co^{4+} and the generation of oxygen vacancy will lead to the lattice expansion. As a result, the substitution of Ti for Co in BSCT can apparently decrease the electronic spin state transition of Co^{3+} ions and reduce the Co^{3+} and oxygen vacancy concentrations, thus consequently resulting in the lower thermal expansion coefficient.

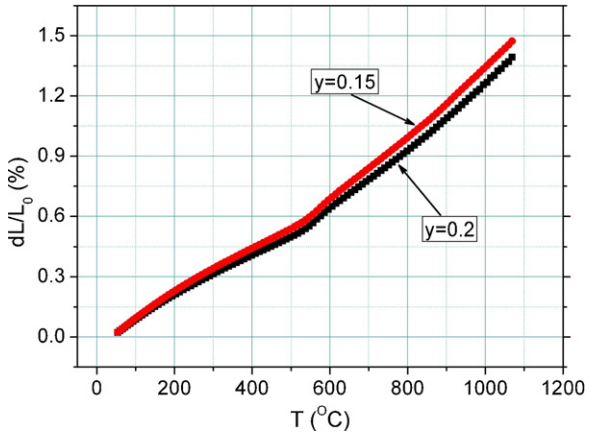

Fig. 6. Thermal expansion curves for $Ba_{0.6}Sr_{0.4}Co_{1-y}Ti_yO_{3-\delta}$ ($y = 0.15$ and 0.2).

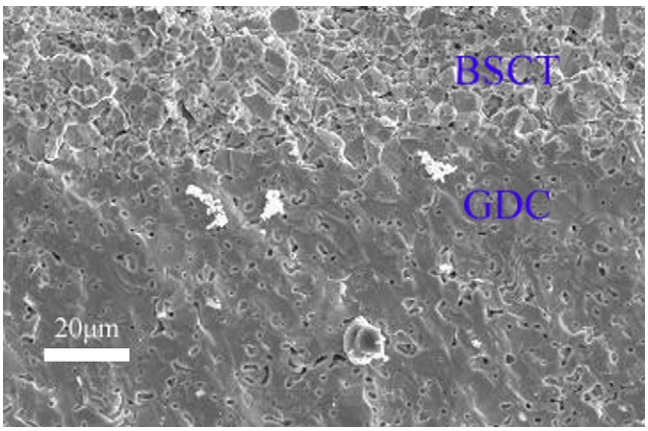

Fig. 7. SEM micrograph of cross-sectional view of GDC/$Ba_{0.6}Sr_{0.4}Co_{0.8}Ti_{0.2}O_{3-\delta}$ interface.

3.4. Physical and chemical compatibility with GDC electrolyte

To assess the physical compatibility of BSCT with GDC electrolyte, $Ba_{0.6}Sr_{0.4}Co_{0.8}Ti_{0.2}O_{3-\delta}$ was screen-printed on the GDC electrolyte, followed by firing at 900°C for 5 h. The SEM micrograph of cross-section of $Ba_{0.6}Sr_{0.4}Co_{0.8}Ti_{0.2}O_{3-\delta}$ layer on GDC electrolyte after firing is shown in Fig. 7. Good adhesion between the $Ba_{0.6}Sr_{0.4}Co_{0.8}Ti_{0.2}O_{3-\delta}$ layer and electrolyte was observed and no apparent cracks were present between them, which is attributed to the similar TEC of BSCT with GDC. Furthermore, the X-ray powder diffraction patterns of $Ba_{0.6}Sr_{0.4}Co_{0.8}Ti_{0.2}O_{3-\delta}$ and GDC mixtures after heating at different temperatures for 5 h indicated no interfacial reaction between the BSCT cathode material and GDC electrolyte below 900 °C (Fig. 8). However, a small amount of impurity was detected in 950 °C-heated samples.

3.5. Single cell performance

GDC electrolyte supported single-cells were prepared to evaluate the cathode performance of $Ba_{0.6}Sr_{0.4}Co_{1-y}Ti_yO_{3-\delta}$. Fig. 9(a, b) shows the performances of the Pt |GDC| BSCT single cells, with humidified hydrogen as fuel and stationary air as oxidant. The open-circuit voltages of the tested half-cells were lower than the theoretical values, and decreased with increasing temperature, as presented in Fig. 9(a). This is mainly due to the electronic conduction characteristics of CeO_2-based electrolyte, which originates from the generation of Ce^{3+} ions in reducing atmosphere and at high temperatures.

The power densities increased obviously with the operating temperature, mainly because of the decreased electrolyte resistance and the improved electrical conductivity and catalytic activity of the cathode materials at high temperatures (Fig. 9a). In order to assess the effect of Ti content on the cathode performance of $Ba_{0.6}Sr_{0.4}Co_{1-y}Ti_yO_{3-\delta}$, Pt |GDC| $Ba_{0.6}Sr_{0.4}Co_{1-y}Ti_yO_{3-\delta}$ single cells were prepared under the same processing condition to ensure the similar inner-structures of single-cells. The power densities decreased with Ti content in $Ba_{0.6}Sr_{0.4}Co_{1-y}Ti_yO_{3-\delta}$, which is considered to be caused by the low electrical conductivity when more Ti was added to the B-site (Fig. 3). The lower electrical conductivity would result in higher electrode polarization, thus affecting the power output of cells. Besides, the decreased electrocatalytic activity due to different surface chemistry could also be the cause of the increase in electrode polarization with increasing Ti content. Fortunately, the decrease in power density was not remarkable (Fig. 9b), but the improvement for TEC of BSCT was significant. It is reasonable to state that BSCT is a potential cathode material for GDC-based IT-SOFC. The maximum power density (MPD) of 74.04 mW cm^{-2} of these cells was obtained when $y = 0.15$ at 800 °C, which is apparently lower than the reported value of SOFCs with BSCF cathode. This is the electrolyte supported characteristics. The thick electrolyte caused large ohmic loss across the electrolyte during the operation of SOFCs and thus deteriorated the cell performance. By the optimization of cathode microstructure and the minimization of the electrolyte thickness, the power density of the cell with BSCT as cathode material could be improved further.

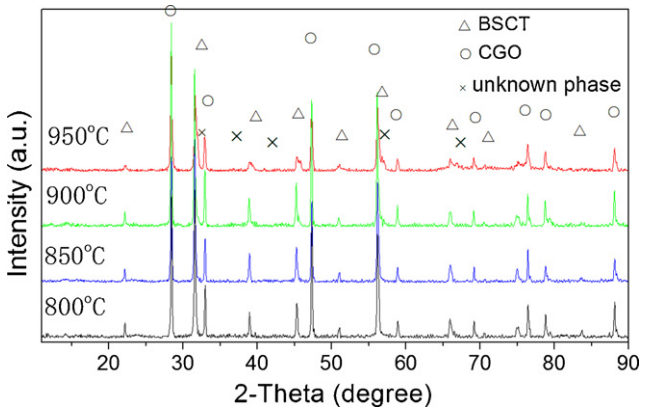

Fig. 8. XRD patterns of $Ba_{0.6}Sr_{0.4}Co_{0.8}Ti_{0.2}O_{3-\delta}$ and GDC mixture co-fired at different temperatures.

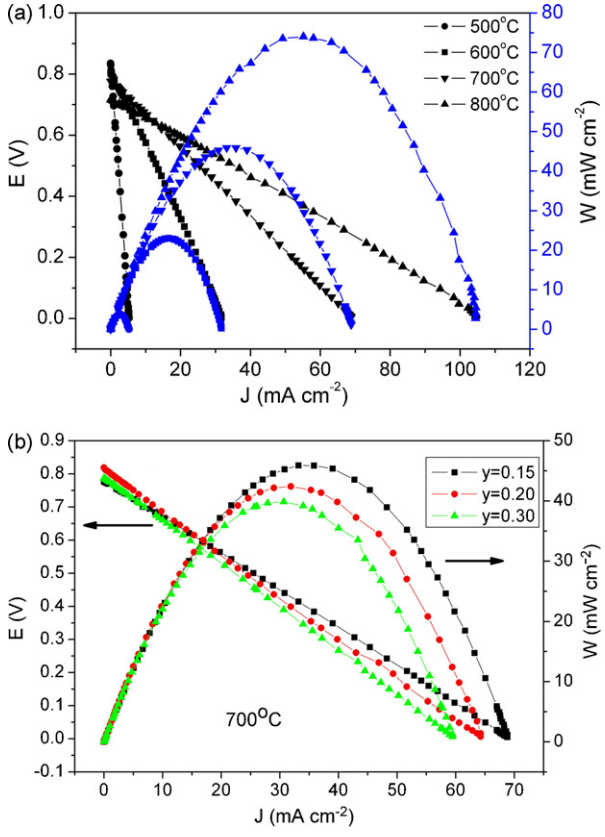

Fig. 9. Performances of the Pt |GDC| BSCT cathode single cell: *I–V* and *I–P* curves for $y = 0.15$ at different temperatures (a) and for BSCT with different Ti contents at 700 °C (b).

4. Conclusions

Cubic perovskite-type $Ba_{0.6}Sr_{0.4}Co_{1-y}Ti_yO_{3-\delta}$ (BSCT, $y = 0.15$–0.3) was successfully synthesized and characterized as a novel cathode for IT-SOFCs. The conductivity of BSCT increased steadily when heating up in the temperature range from 300 to 900 °C with an electrical conductivity fluctuation at about 550 °C where lattice oxygen was lost and oxygen vacancies thus being formed. Ti addition can minimize the lattice oxygen loss and thus increase the structure stability of BSCT. BSCT exhibited a small polaron conduction behavior and the electrical conductivity decreased with Ti content due to the decreased charge carrier concentration, $[Co^{\bullet}_{Co}]$. The TEC values for BSCT materials were $\sim 14 \times 10^{-6}\ K^{-1}$ in the temperature range of 50–1050 °C, which were very close to that of GDC electrolyte. BSCT materials had good thermal cyclic stability of conductivity, and good physical and chemical compatibility with GDC electrolyte below 900 °C. Incorporation of Ti in BSCT decreased the cathode performance slightly but improved the TEC values remarkably. Using BSCT as cathode, GDC as supported electrolyte, the single cell exhibited maximum power density of 74.04 mW cm^{-2} when $y = 0.15$ at 800 °C. Further modification of the cathode composition and optimization of the cell structure could result in improved performance, making BSCT a prospective cathode material for the IT-SOFCs based on doped ceria electrolytes.

Acknowledgements

This research was kindly supported by the National Natural Science Foundation of China (No. 50672009) and 863 Program of National High Technology Research Development Project of China (No. 2006AA11A189).

References

[1] N.Q. Minh, J. Am. Ceram. Soc 76 (3) (1993) 563–588.
[2] T.H. Estell, S.N. Flengas, Chem. Rev. 70 (1970) 339–376.
[3] B.C.H. Steele, Curr. Opin. Solid State Mater. Sci. 1 (1996) 684–691.
[4] B.C.H. Steele, Solid State Ionics 129 (2000) 95–110.
[5] R. Doshi, V.L. Richards, J.D. Carter, X. Wang, M. Krumpelt, J. Electrochem. Soc. 146 (1999) 1273–1278.
[6] Y. Jiang, S.Z. Wang, Y.H. Zhang, J.W. Yan, W.Z. Li, J. Electrochem. Soc. 145 (1998) 373–378.
[7] C.R. Xia, W. Rauch, F.L. Chen, M.L. Liu, Solid State Ionics 149 (2002) 11–19.
[8] M.J. Jorgensen, S. Primdahl, M. Mogensen, Electrochim. Acta 44 (1999) 4195–4201.
[9] M.J.L. Ostergard, C. Clausen, C. Bagger, M. Mogensen, Electrochim. Acta 40 (1995) 1971–1981.
[10] Z. Lei, Q. Zhu, L. Zhao, J. Power Sources 161 (2006) 1169–1175.
[11] T. Tsai, S.A. Barnett, Solid State Ionics 93 (1997) 207–217.
[12] S.P. Jiang, W. Wang, J. Electrochem. Soc. 152 (2005) 1398–1408.
[13] X.D. Zhu, K.N. Sun, N.Q. Zhang, X.B. Chen, L.J. Wu, D.C. Jia, Electrochem. Commun. 9 (2007) 431–435.
[14] C.R. Xia, M.L. Liu, Solid State Ionics 144 (2001) 249–255.
[15] X. Zhang, M. Robertson, S. Yick, C. Deĉes-Petit, E. Styles, W. Qu, Y. Xie, R. Hui, J. Roller, O. Kesler, R. Maric, D. Ghosh, J. Power Sources 160 (2006) 1211–1216.
[16] V. Dusastre, J.A. Kilner, Solid State Ionics 126 (1999) 163–174.
[17] Z. Shao, S.M. Haile, Nature 431 (2004) 170–173.
[18] S. Lee, Y. Lim, E.A. Lee, H.J. Hwang, J.-W. Moon, J. Power Sources 157 (2006) 848–854.
[19] Z. Duan, M. Yang, A. Yan, Z. Hou, Y. Dong, Y. Chong, M. Cheng, W. Yang, J. Power Sources 160 (2006) 57–64.
[20] J. Peña-Martínez, D. Marrero-López, J.C. Ruiz-Morales, B.E. Buergler, P. Núñez, L.J. Gauckler, Solid State Ionics 177 (2006) 2143–2147.
[21] Q.L. Liu, K.A. Khor, S.H. Chan, J. Power Sources 161 (2006) 123–128.
[22] B. Wei, W. Su, Z. Lü, X. Huang, S. Li, G. Ai, Z. Liu, Mater. Lett. 60 (2006) 3642–3646.
[23] Q. Zhu, T. Jin, Y. Wang, Solid State Ionics 177 (2006) 1199–1204.
[24] B. Wei, Z. Lü, X. Huang, J. Eur. Ceram. Soc. 26 (2006) 2827–2832.
[25] S. McIntosh, J.F. Vente, W.G. Haije, D.H.A. Blank, H.J.M. Bouwmeester, Chem. Mater. 18 (2006) 2187–2193.
[26] J. Peña-Martínez, D. Marrero-López, J.C. Ruiz-Morales, B.E. Buergler, P. Núñez, L.J. Gauckler, J. Power Sources 159 (2006) 914–921.
[27] K. Huang, H.Y. Lee, J.B. Goodenough, J. Electrochem. Soc. 145 (1998) 3220–3227.
[28] K.T. Lee, A. Manthiram, Solid State Ionics 178 (2007) 995–1000.
[29] H. Zhao, W. Shen, Z. Zhu, X. Li, Z. Wang, J. Power Sources 182 (2008) 503–509.
[30] M. Parras, A. Varela, H. Seehofer, J.M. Gonzalez-Calbet, J. Solid State Chem. 120 (1995) 327–331.
[31] N. Bonanos, K.S. Knight, B. Ellis, Solid State Ionics 79 (1995) 161–170.
[32] Y. Cheng, H. Zhao, D. Teng, F. Li, X. Lu, W. Ding, J. Membr. Sci. 322 (2008) 484–490.
[33] A.F. Sammells, R.L. Cook, J.H. White, J.J. Osborne, R.C. MacDuff, Solid State Ionics 52 (1992) 111–123.
[34] R.D. Shannon, Acta. Cryst. A32 (1976) 751–767.
[35] G.Ch. Kostogloudis, Ch. Ftikos, Solid State Ionics 135 (2000) 537–541.
[36] L.W. Tai, M.M. Nasrallah, H.U. Anderson, D.M. Sparlin, S.R. Sehlin, Solid State Ionics 76 (1995) 259–271.
[37] J.W. Stevenson, T.R. Armstrong, R.D. Carneim, L.R. Pederson, W.J. Weber, J. Electrochem. Soc. 143 (1996) 2722–2729.
[38] Z. Chen, R. Ran, W. Zhou, Z. Shao, S. Liu, Electrochim. Acta 52 (2007) 7343–7351.
[39] K.J. Moreno, G. Mendoza-Suárez, A.F. Fuentes, Phys. Rev. B 71 (2005) 132301.
[40] L. Ge, W. Zhou, R. Ran, S. Liu, Z. Shao, W. Jin, N. Xu, J. Membr. Sci. 306 (2007) 318–328.
[41] H. Hayashi, M. Kanoh, C.J. Quan, Solid State Ionics 132 (2000) 227–233.